EARTHQUAKE ENGINEERING AND STRUCTURAL DYNAMICS, VOL. 24, 313–324 (1995)

INVESTIGATION OF NON-LINEAR SITE AMPLIFICATION AT TWO DOWNHOLE STRONG GROUND MOTION ARRAYS IN TAIWAN

KUO-LIANG WEN,* IGOR A. BERESNEV† AND YEONG TEIN YEH‡
Institute of Earth Sciences, Academia Sinica, P.O. Box 1-55, Nankang, Taipei 11529, Taiwan

SUMMARY

Non-linear seismic response of soil is studied by comparing the spectral ratios of surface to downhole horizontal accelerations on weak and strong motion. Data from two boreholes are analysed. One is drilled in the alluvial deposits in the south–west quadrant of the SMART1 array. The second one penetrates Pleistocene terrace deposits in the northern part of the SMART2 array. Observed weak and strong motion spectral ratios are compared with the theoretical ones predicted by the geotechnical soil model which postulates a hysteretic constitutive law. A significant non-linear response is found at the first site for the events with surface peak acceleration exceeding roughly 0·15*g*. Deamplification of the strong motion occurred in the frequency range from approximately 1 to 10 Hz. The maximum observed difference between the average weak and strong motion amplification functions of an 11 m-thick near-surface stratum is a factor of 2·3. Non-linear response characteristics are in qualitative agreement with the model. An additional corollary is that the amplification function calculated from the shear wave coda is equivalent to the average amplification calculated over the ensemble of small earthquakes. No statistically significant non-linear response is detected on the second array, that is tentatively accounted for by the stiffer soil conditions and weaker accelerations achieved at the SMART2 site. The results indicate that the non-linear amplification can be detectable at certain soil conditions above a threshold acceleration level.

INTRODUCTION

Non-linear soil response in strong ground motion caused by earthquakes has long been a controversial subject in seismology and earthquake engineering. It has been known theoretically since the pioneering works carried out by Idriss and Seed[1] that non-linear effects in near-surface deposits can be manifested in increased damping and reduced shear wave velocity (V), both occurring as the excitation strength increases from low to high. Since $V = 4Hf$, where f is the fundamental frequency of the surface layer and H is its thickness,[2] the decrease in shear wave velocity should be associated with the downward shift in the resonance frequency of the layer. The above non-linear effects are caused by the typically hysteretic nature of soil shearing deformation, as revealed from vibratory and cycling loading tests performed on soil samples under laboratory conditions.[3–5] A threshold acceleration level beyond which there is an appreciable departure of the ground response from linear prediction, expected in geotechnical engineering, is approximately 100–150 Gal (cm/s^2).[1,6–8]

It is also known that low-impedance superficial layers amplify the upcoming seismic waves.[2,9,10] As non-linear effects increase the effective damping in soils, they work against the common amplification. Thus, one of the characteristic symptoms of non-linear ground response is deamplification of strong motion compared with the weak motion.

Reliable demonstrations of the non-linear ground response derived from seismological data did not exist until very recently and seem to be scarce. That is why non-linearity was never taken seriously in seismological

*Associate Research Fellow.
†Visiting Specialist.
‡Research Fellow.

CCC 0098–8847/95/030313–12

Received 28 March 1994
Revised 4 July 1994

practice, while being widely recognized in the geotechnical engineering community.[11,12] This controversy raises the problem of direct seismological substantiation of non-linear site effects. First such an evidence appeared after high-quality digital recordings from recent major earthquakes became available. Strong motion deamplification effects were observed for the aftershocks of the 1983 Coalinga (California) earthquake,[13] during the 1985 Michoacan (Mexico) earthquake[14] and the 1989 Loma Prieta (California) earthquake.[8,15]

A main obstacle to identifying non-linear site effect is that observed spectra are contaminated by source and path spectral contributions. A straightforward way to reduce these effects and to obtain an approximation of the frequency-dependent site amplification function is to take the ratio of Fourier amplitude spectrum at one site to that at a reference site. As a rule, a station installed on a hard rock outcrop is chosen as a reference station, which is assumed to reproduce an input seismic motion.[2,14–17] However, this procedure never fully eliminates spurious source and path contributions because of the finite distance between the stations, which rarely is less than several kilometers. Inherent deviation of the spectral ratio from the pure site response is then caused by the differences in the source radiation and the wave propagation path towards two stations.

The latter problem is overcome efficiently when the site amplification function is assessed using the uphole/downhole data. The distance between the recording instruments is negligibly small compared with the distance to the earthquake source in this case, so that the site response can be almost ideally isolated by taking the spectral ratio of the surface to downhole accelerations.[18,19]

Non-linear site effects in the upward vertically propagating transverse wave have been theoretically modelled recently in Reference 20. A hysteretic stress–strain relationship with a hyperbolic skeleton curve was postulated, and calculations of the transfer functions were performed in the linear and non-linear cases using a public-domain geotechnical code DESRA2.[21] Predicted spectral ratios of accelerations between the surface and the centre of a soil layer having a thickness of 20 m are reproduced in Figure 1.

Numerical simulation revealed that non-linear soil response does not come to a mere deamplification effect and has frequency-dependent features. It can be separated into three frequency bands. Ratios are not affected by non-linearity at the low-frequency band, because the wavelength is sufficiently long for the waves not to 'see' the sub-surface layer. In the central frequency range, non-linear deamplification occurs. Finally, spectral ratios in the strong motion are, conversely, amplified over those in weak motion in the high-frequency band, owing to the non-linear generation of multiple and sum harmonics (similar to that observed with sinusoidal and braodband seismic signals in References 22 and 23, respectively). A shift of the fundamental frequency from, approximately, 5·0 to 2·8 Hz in the non-linear response is clearly seen in Figure 1. We verify the non-linear phenomena outlined in this prediction using the weak and strong motion data recorded by two

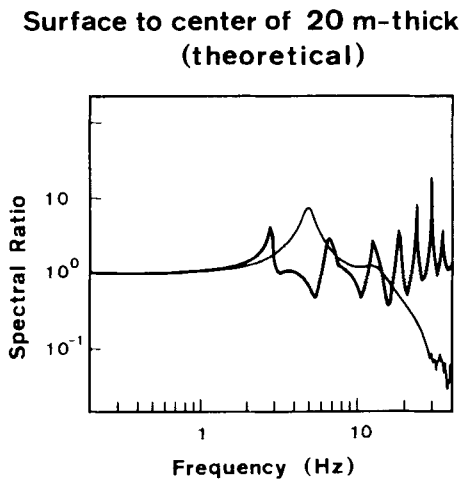

Figure 1. Theoretical spectral ratios of accelerations at the surface to the centre of a soil layer in linear (thin line) and non-linear (bold line) responses (after Reference 20)

downhole strong motion arrays installed in the different sedimentary units. Mixed results have been obtained. One borehole clearly displays the symptoms of non-linear behaviour, while the response of the other one remains linear in the acceleration range considered.

DATA AND METHOD

Our data consist of the recordings from two downhole accelerograph arrays deployed in Taiwan.

LSST array

One borehole is drilled to a depth of 47 m in the alluvial deposits at the LSST (Lotung Large-Scale Seismic Test) site in the south–west quadrant of the SMART1 array[24,25] (Figure 2). The sediments are mostly composed of interlayered silty sand and silty clay beds with gravel;[26] their shear wave velocity profile measured by uphole and cross-hole shooting methods is given in Figure 3. This site is geotechnically classified as 'deep cohesionless soil site'.[27,28] Accelerographs are installed at the surface and the depths of 6, 11, 17 and 47 m. Digital data were recorded as 12-bit words at the rate of 200 samples per second. We present the spectral ratios obtained between the surface and 11 or 47 m in this paper.

LSST array was operational in 1985–1988. Parameters of the events selected for the analysis are listed in Table I; the map of their epicenters is shown in Figure 4, where the triangle stands for the downhole array, and the circle size is proportional to the magnitude of earthquake. Earthquakes having Peak Ground Acceleration (PGA) at the surface less than 60 Gal are attributed to the 'weak motion' class. Events with PGA over 150 Gal (roughly $0{\cdot}15g$) are considered 'strong motions'. Maximum acceleration recorded is about 224 Gal. The transition between the two classes roughly corresponds to the acceleration level beyond which appreciable non-linear effects can be expected from the geotechnical calculations.

Note that we use the value of peak ground acceleration to quantify roughly earthquakes as weak and strong ones, and not to characterize the soil amplification. PGA value does not reflect the actual frequency content of

Table I. Selected LSST events

Event	Date	Depth (km)	M_L	Δ* (km)	$PGA_0/PGA_{11}/PGA_{47}^{\dagger}$ (Gal)
Weak motion					
3	07/11/85	74	5·5	17	27·3/12·0/9·3
5	29/03/86	10	4·7	8	41·4/17·8/15·4
6	08/04/86	11	5·4	31	35·4/15·2/13·0
8	20/05/86	22	6·2	69	35·0/21·5/14·2
14	30/07/86	2	4·9	5	57·5/31·2
20	10/12/86	98	5·8	42	23·8/11·4
21	06/01/87	28	6·2	77	31·8/16·8
22	04/02/87	70	5·8	16	43·4/20·4
23	24/06/87	31	5·7	52	31·7/11·5
24	27/06/87	1	5·3	40	23·7/13·1
27	18/09/88	63	5·6	68	22·3/11·1
Strong motion					
7	20/05/86	16	6·5	66	223·6/113·7/96·9
12	30/07/86	2	6·2	5	186·7/192·8
16	14/11/86	7	7·0	78	167·2/94·6
Foreshocks to event 12					
9	11/07/86	1	4·5	5	72·8/34·1/28·4
10	16/07/86	1	4·5	6	70·0/26·3/19·2

*Epicentral distance.

†Peak horizontal acceleration at the surface, 11 and 47 m, respectively. Recordings at 47 m are not available at the earthquakes subsequent to No. 10.

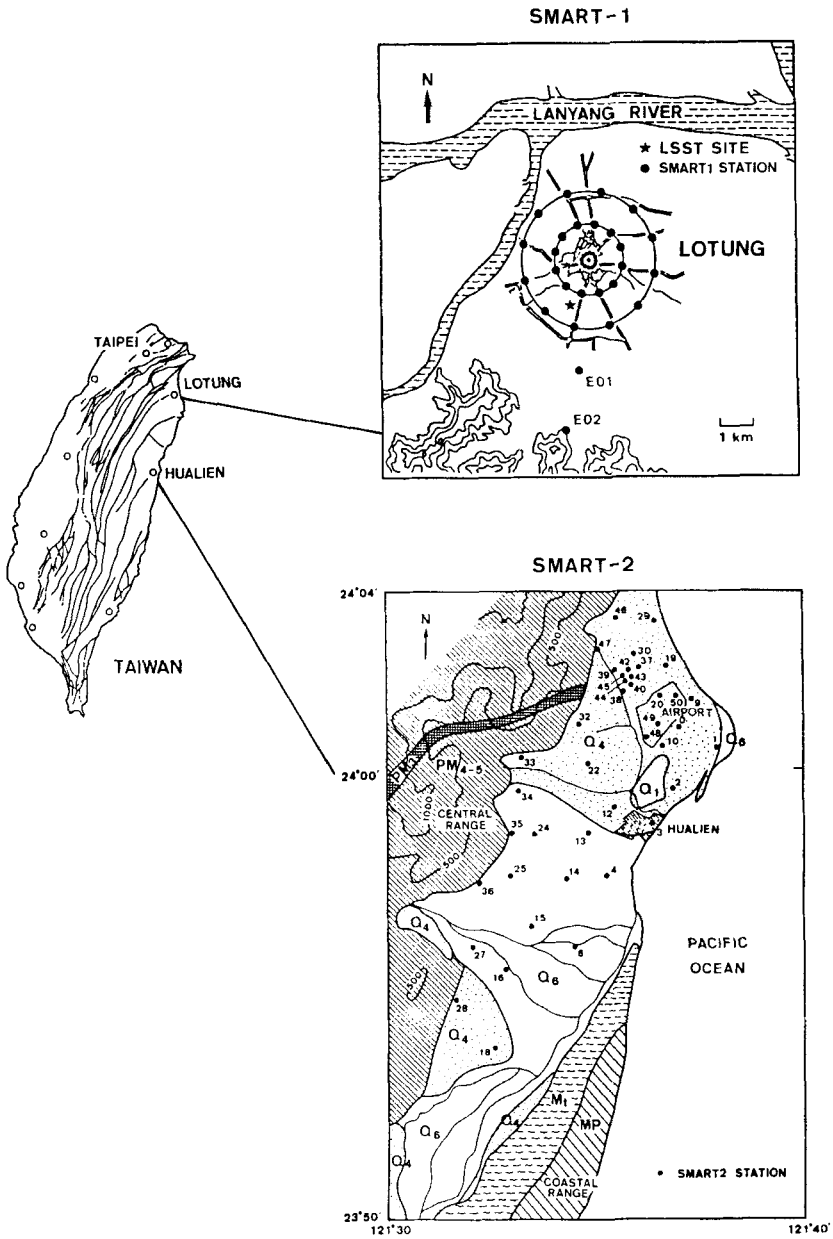

Figure 2. Location and layout of the SMART1 and SMART2 arrays. Q_6 is the recent alluvium, Q_4 is Pleistocene terrace deposits (gravel, sand, clay), Q_1 is older Pleistocene sediments, MP is Late-Miocene to Pliocene rock, Mt is early Miocene rock, PM_{4-5} is Late Paleozoic to Mesozoic schist, and PM_3 is Late Paleozoic to Mesozoic limestone

the field which, as Figure 1 shows, is crucial in characterizing the non-linear amplification effect. For example, deamplification, overamplification, or equal amplification (relative to the weak motion) may occur for the strong events with even identical PGA, depending on which of three frequency bands their predominant energy falls into. The use of PGA may be therefore misleading, whereas the comparison of spectral ratios gives a correct understanding.

Wen[25] analysed shear wave velocity reduction effects which occurred at the LSST array as a consequence of non-linear response. In this article, we focus on the observed differences in weak and strong motion amplification.

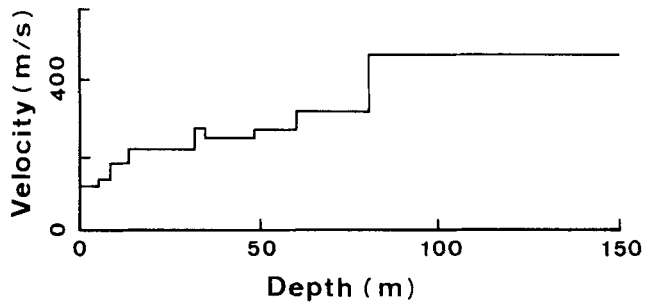

Figure 3. Shear wave velocity structure at the LSST borehole

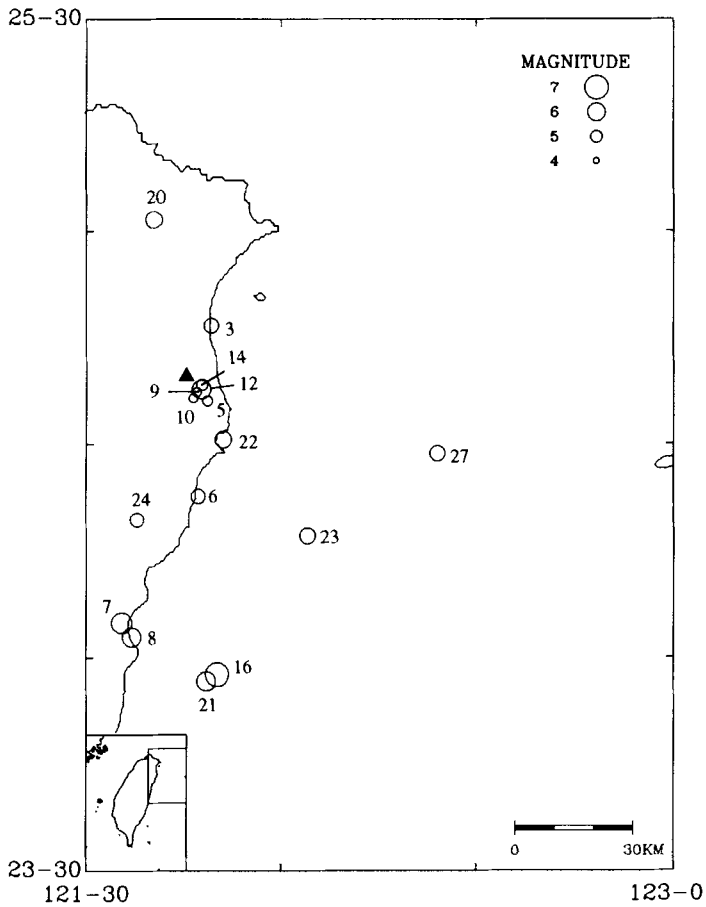

Figure 4. Epicentres of LSST earthquakes

SMART2 array

The second borehole is situated in the northern part of the SMART2 array which is currently deployed in the eastern coast of Taiwan.[29] All of the SMART2 stations are located in the sedimentary valley bordering upon the Central Range in the west and the Coastal Range or the Pacific coast in the east (Figure 2). Downhole array started operation in 1992. The borehole is drilled at the location of the station 37 through the Pleistocene terrace deposits composed of sand, mud, and gravel to a depth of 200 m. Figure 5 gives its shear wave velocity structure.[30] Accelerographs are emplaced at the surface and the depths of 50, 100 and 200 m.

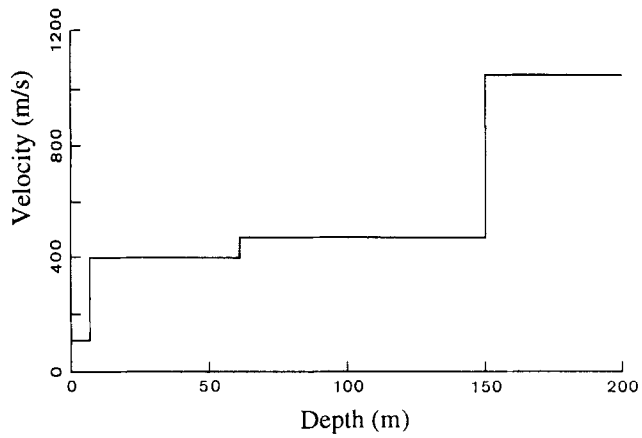

Figure 5. Shear wave velocity structure at the SMART2 borehole

We will address the surface to 200 m spectral ratios below in order to illustrate the amplification induced by the entire penetrated soil column. All the accelerometers have a 16-bit resolution; the ground motion is digitized at 200 samples per second.

Characteristics of the selected SMART2 events are given in Table II; their epicentres are indicated on the map in Figure 6. The distinction between the 'weak' and 'strong' events is slightly different from that described previously. The earthquake was attributed to the 'weak motion' class if the maximum horizontal acceleration did not surpass 20 Gal. 'Strong' events had surface PGA at both EW and NS components exceeding 100 Gal. The difference with the LSST case is due to the higher precision of the SMART2 instruments, which allowed to lower their triggering level. Maximum acceleration achieved is 160 Gal.

Table II. Selected SMART2 events

Event	Date	PGA_0/PGA^*_{200} (Gal) EW	NS	M_L	Depth (km)	Hypocentral distance (km)
Weak motion						
176	21/5/92	15·4/1·7	11·6/3·4	4·5	16·7	38·4
185	30/6/92	17·5/4·9	16·5/4·2	4·5	28·6	33·9
189	23/7/92	11·2/2·5	15·3/3·0	4·5	12·8	31·1
198	9/10/92	16·5/2·3	5·1/2·9	4·1	15·9	24·1
222	4/5/93	10·3/2·0	17·5/2·6	4·0	1·0	5·8
231	24/6/93	11·5/1·9	12·0/2·6	5·2	65·0	87·4
234	25/6/93	17·5/4·1	15·0/3·2	3·9	4·6	12·2
235	26/6/93	17·0/4·1	12·8/3·1	3·6	6·7	11·6
Strong motion						
183	25/6/92	160·2/34·8	93·7/28·3	4·5	22·7	24·2
192	14/8/92	135·9/50·6	108·6/31·7	4·5	15·7	26·3
202	28/12/92	117·6/24·8	154·4/23·4	4·9	16·2	32·4
Aftershock, coda						
184	25/6/92	38·3/7·5	24·6/7·7	3·3	13·4	23·3
183coda†		16·5/4·9	15·3/3·8			
192coda†		11·5/3·4	8·8/3·6			
202coda†		13·1/2·5	8·7/3·4			

*Peak horizontal acceleration at the surface and 200 m, respectively.
†Eight-seconds-long coda following shear wave window.

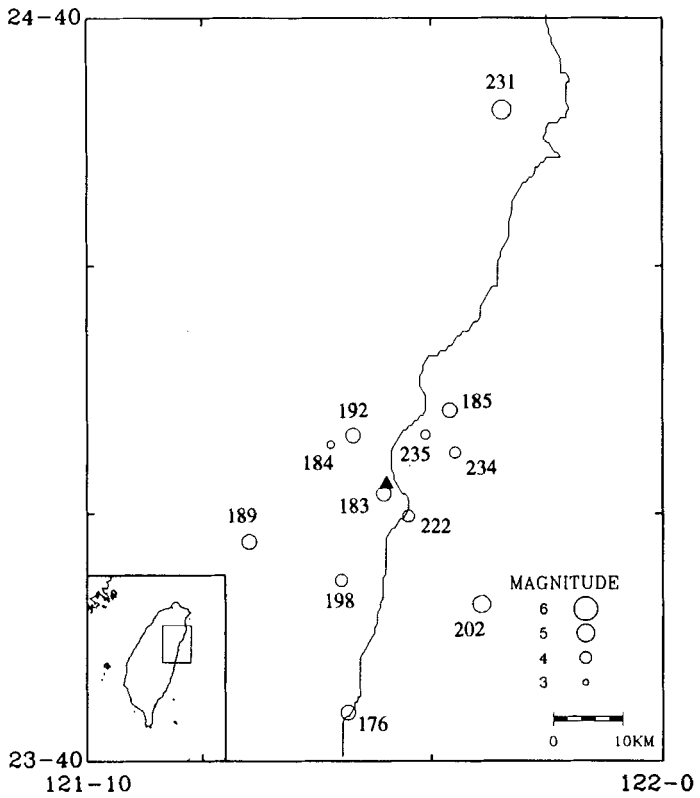

Figure 6. Epicentres of SMART2 earthquakes

Method of spectral ratio calculation

Horizontal axes of downhole instruments at the SMART2 array deviate from the EW and NS directions by 75° clockwise in the horizontal plane.[30] Correspondingly, the accelerograms were rotated back to the EW and NS directions before calculations were started. LSST array instruments are in the right position since installation.

Spectral ratios are calculated using the following technique: (1) an 8 s window containing the shear wave is identified; (2) the window is tapered using a 5-per cent-of window-length half-bell cosine function; (3) the Fourier amplitude spectrum is calculated; (4) the spectrum is smoothed using a three-point running Hanning average filter having a bandwidth of approximately 0·1 Hz; (5) the ratio of two smoothed spectra is then calculated. Eighty and ten consecutive smoothings were applied to the raw spectra of the LSST and SMART2 recordings, respectively. These numbers were chosen empirically considering their visual effect on the spectral shape. All curves plotted below are the average horizontal spectral ratios calculated by summing the squares of the ratios for EW- and NS-components, dividing by two, and taking the square root.

A signal-to-noise ratio was estimated from the accelerograms having sufficiently long pre-event noise time history by dividing the smoothed amplitude spectra of the S-wave and the pre-event noise. All results are plotted in the frequency bands where the signal-to-noise ratio is greater than five.

RESULTS

LSST array

Figure 7 compares the average spectral ratios calculated for eleven weak and three strong LSST events as they appear in Table I (thin and bold lines, respectively). The shaded bands around the average curves represent ± 1 standard deviation. Ratios of spectra at surface to 11 and 47 m are shown in Figures 7(a) and

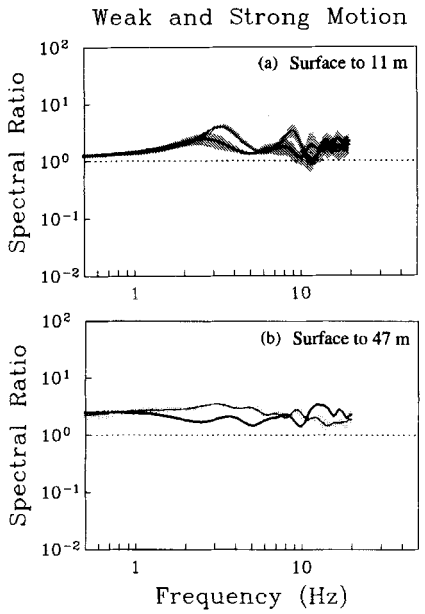

Figure 7. Comparison of the average spectral ratios calculated on weak motion (thin lines) and strong motion (bold lines) at the LSST array

7(b), respectively. The strong motion ratio is given only for event 7 in Figure 7(b), because the instrument at this depth has been unoperational since event 11 was recorded.

It can be seen, firstly, that the soil column amplifies the weak motion at all frequencies. The fundamental frequency of the upper 11 m of the soil is approximately 3·5 Hz as seen in Figure 7(a). The standard deviation of the weak motion spectral ratios between the frequencies from approximately 0·5 to 12 Hz has a small value of about 0·07 log units, which corresponds to a factor of 1·2. This implies that weak motion transfer functions are estimated rather precisely by taking the ratio of uphole to downhole acceleration spectra.

Secondly, reduction in strong motion ratios is clearly observed in the intervals from, approximately, 2·5 to 5·5, and 8 to 10 Hz in Figure 7(a), and 1 to 7, and 8·5 to 10 Hz in Figure 7(b), suggesting a non-linear response in agreement with the theoretical prediction. Effect of the downward shift in the fundamental frequency from 3·5 to about 2·7 Hz is also seen for the upper 11 m in Figure 7(a). The deamplification effect well exceeds the error margin imposed by the standard deviations. Maximum average deamplification by a factor of about 2·3 occurs in Figure 7(a) at approximately 3·7 and 9 Hz. For instance, at the frequency of the second resonance near 9 Hz, the weak motion amplification is 3·4 versus only 1·5 in the strong motion. Spectral ratios converge at the low-frequency limit, as also anticipated from the theory. However, predicted relative amplification of the strong motion over the weak motion in the high frequencies emerges solely in Figure 7(b) where only a strong event 7 is shown. We address this discrepancy in more detail in a later section.

Figure 8 presents spectral ratios for the same two pairs of instruments taken individually for the strong earthquake 7 (bold lines) and its aftershock 8 (thin lines). The aftershock took place approximately 11 min after the main shock and had a close hypocentre. Peak horizontal accelerations at the surface were 224 and 35 Gal for the main shock and the aftershock, respectively. Characteristic frequency bands, in which the linear and non-linear responses diverge, appear on these plots. Namely, strong motion deamplification occurs in roughly the same frequency range as in Figure 7. A high-frequency interval where the strong motion is relatively amplified is clearly seen in both Figures 8(a) and 8(b) above approximately 10 Hz. Behaviour of overall curves in Figure 8 compares well with the calculation in Figure 1.

Figure 9 similarly compares spectral ratios for the strong earthquake 12 (bold line) and its foreshocks and aftershocks (events 9, 10 and 14 in Table I) calculated for the one pair of instruments. Also plotted in Figure 9 is a weak motion ratio obtained from the coda part of the event 12 time history. An eight-second coda window

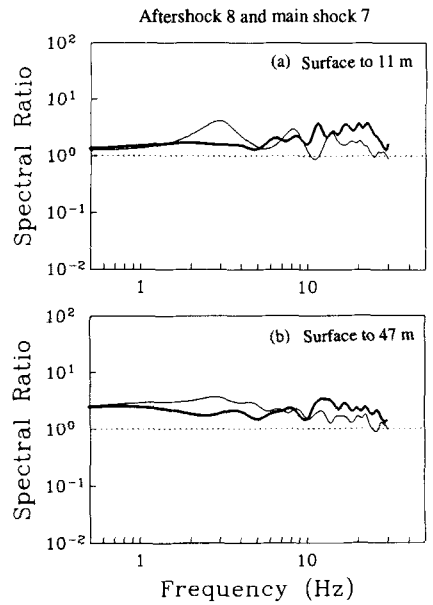

Figure 8. Spectral ratios calculated for the strong shock 7 (bold lines) and its aftershock 8 (thin lines) at the LSST array

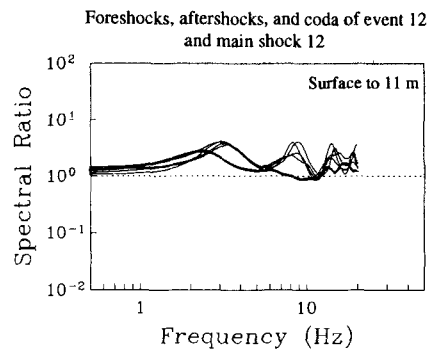

Figure 9. Spectral ratios between the surface and a depth of 11 m for the strong shock 12 (bold line), and its foreshocks, aftershocks and coda (thin lines)

starting at 17 s after the S-wave arrival was used. One can see that all spectral ratios calculated from foreshocks, aftershocks, and coda match well (thin lines). They have fundamental frequencies between 3 and 3·5 Hz. The symptoms of non-linear behaviour consist in that the strong motion ratio is markedly reduced between approximately 2·6 and 11 Hz except for the narrow interval in the vicinity of 6 Hz, as well as in that its fundamental frequency decreases to about 2·3 Hz. However, high-frequency non-linear amplification effect is not manifested in Figure 9. As inferred from the previous analysis, only earthquake 7 exhibited this effect. The explanation for such an inconsistency is not apparent at this time. One possible reason is that the event 7 produced a largest horizontal acceleration of about 0·22g, that may have resulted in a more pronounced non-linear response than in the other earthquakes.

A corollary drawn from Figure 9 is that amplification function calculated from the coda of a strong shear wave is a good approximation of the average weak motion amplification function. This fact suggests that the ground motion in the coda is not affected by the earlier hysteretic shaking in that particle motion recurs to a seemingly linear elastic regime after its termination.

SMART2 array

The same comparison of the weak and strong motion amplification functions was carried out for the data from the SMART2 downhole array. Figure 10 demonstrates the average spectral ratios, where the thin line is the mean of eight weak motion and three coda ratios, while the bold line is the mean of three strong motion ratios (Table II). Figure 11 shows the ratios obtained for the strong quake 183 and its aftershock 184, which have peak accelerations of 160 and 38 Gal, respectively. Aftershock followed in approximately 68 min after the main shock. All ratios are between the surface and 200 m accelerometers.

Figure 10 indicates that ground motion amplification induced by a 200 m-thick upper soil layer is notably larger than that obtained for the thinner strata at the LSST array. Average weak motion amplification peak around 9 Hz reaches a value of about 10. However, Figures 10 and 11 demonstrate that there is no statistically significant deviation of the strong motion amplification function from that on weak motion in the acceleration range considered. The same applies to the surface to 50 m spectral ratios which we do not adduce herein.

To check whether event 183 in Figure 11 has a significant energy content at the lower frequencies where the non-linear deamplification effect is likely to take place, we examine its amplitude spectrum corresponding to the record of a surface accelerometer. This spectrum, obtained as an arithmetic average of the spectra of the EW- and NS-components in the S-wave window, is shown in Figure 12. It is relatively flat between approximately 2 and 11 Hz, showing that a non-uniform energy distribution in the frequency domain is unlikely to explain the almost linear soil behaviour found in the ratios in Figure 11.

This result is in contradiction with the observation made at the LSST site. Two tentative explanations to this effect can be propounded. Firstly, the average surface horizontal PGA in three strong LSST events is 193 Gal, compared with 150 Gal in the SMART2 data. This difference could be a cause of a larger non-linear

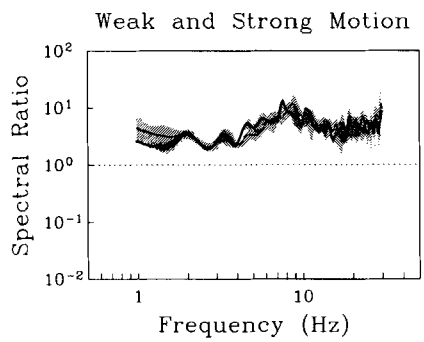

Figure 10. Average weak motion and strong motion spectral ratios at the SMART2 array (thin and bold line, respectively)

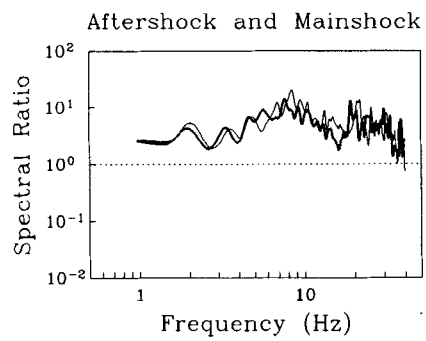

Figure 11. Spectral ratios for the strong shock 183 (bold line) and its aftershock 184 (thin line) at the SMART2 array

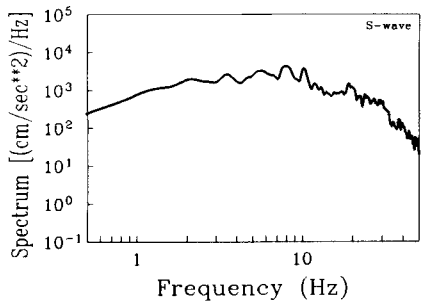

Figure 12. Fourier amplitude spectrum of the surface record of the SMART2 event 183

response occurring at the LSST site. Secondly, as can be concluded from the comparison of Figures 3 and 5, the SMART2 site has higher shear wave velocities and, consequently, stiffer soil conditions between the surface and the depth of approximately 80 m. As it is known from soil engineering practice, the threshold acceleration beyond which the deviation from the linear elasticity begins increases with the soil stiffness (e.g. Figure 10 of Reference 6). This factor can also be accountable for the apparently linear response experienced at the SMART2 array.

DISCUSSION

The objective of this paper is an attempt to answer the question whether the amplitude-dependent site amplification effect can be observable. We compare theoretical and observed soil responses on weak and strong ground motion, using uphole/downhole acceleration data from two vertical arrays. Observations at two sites gave mixed results. Data from the LSST array installed in the 'deep cohesionless' alluvial deposits clearly identify the reduction in soil amplification occurring at surface accelerations exceeding approximately 0·15*g*. Deamplification is accompanied by the decrease in the fundamental frequency of the soil column in accordance with the non-linear hysteretic model of deformation. The maximum observed difference between the average weak and strong motion amplification functions of an 11 m-thick near-surface stratum is a factor of 2·3, occurring at approximately 3·7 and 9 Hz. The existence of a numerically predicted high-frequency amplification of strong motion over the weak motion is also confirmed for the strongest event with the PGA of about 0·22*g*.

On the other hand, an essentially linear ground response is found in the data from the SMART2 vertical array, where accelerations of up to 0·16*g* were recorded. The discrepancy between these two observations is tentatively attributed to the lower peak accelerations achieved and the stiffer soil conditions at the SMART2 array, that could keep the deformations experienced at this site out of the range of detectable non-linearity.

One of the conclusions of this analysis is that spectral ratios derived from shear wave coda in the strong motion accelerograms are identical to the ratios calculated from individual weak earthquakes. This allows one to assess both weak and strong motion amplification functions using a recording of the strong earthquake only.

Results of this investigation show that non-linear soil response in seismic motion can be detectable at certain soil conditions and above a certain threshold acceleration, having the characteristics consistent with the models adopted in geotechnical engineering.

ACKNOWLEDGEMENTS

Permission by Taiwan Power Company (R.O.C.) and the Electric Power Research Institute (U.S.A.) to use the unreleased data of the LSST array is gratefully acknowledged. We thank Dr. H.-C. Chiu and the technical staff of the Institute of Earth Sciences who are in charge of the operation of the SMART2 array. Corrected accelerograms were prepared by W.G. Huang and the data processing group. Review of the manuscript by P.A. Johnson from the Los Alamos National Laboratory, U.S.A., is greatly appreciated. Our thanks go to

Prof. G.B. Warburton and two reviewers of this paper for their constructive comments. This work was supported by the National Science Council, Republic of China, under the grant NSC 83-0202-M-001-004.

REFERENCES

1. I. M. Idriss and H. B. Seed, 'An analysis of ground motions during the 1957 San Francisco earthquake', *Bull. seism. soc. Am.* **58**, 2013–2032 (1968).
2. J. R. Murphy, A. H. Davis and N. L. Weaver, 'Amplification of seismic body waves by low-velocity surface layers', *Bull. seism. soc. Am.* **61**, 109–145 (1971).
3. B. O. Hardin and V. P. Drnevich, 'Shear modulus and damping in soil: measurement and parameter effects', *J. soil mech. found. div. ASCE* **98**, 603–624 (1972).
4. B. Mohammadioun and A. Pecker, 'Low-frequency transfer of seismic energy by superficial soil deposits and soft rocks', *Earthquake eng. struct. dyn.* **12**, 537–564 (1984).
5. M. Erdik, 'Site response analysis', in M. O. Erdik and M. N. Toksöz (eds), *Strong Ground Motion Seismology*, D. Reidel, 1987, pp. 479–534.
6. H. B. Seed, R. Murarka, J. Lysmer and I. M. Idriss, 'Relationships of maximum acceleration, maximum velocity, distance from source, and local site conditions for moderately strong earthquakes', *Bull. seism. soc. Am.* **66**, 1323–1342 (1976).
7. M. Sugito and H. Kameda, 'Nonlinear soil amplification model with verification by vertical strong motion array records', in *Proc. 4th U.S. natl. conf. earthquake eng.*, Palm Springs, CA, Vol. 1, 1990, pp. 555–564.
8. B.-H. Chin and K. Aki, 'Simultaneous study of the source, path, and site effects on strong ground motion during the 1989 Loma Prieta earthquake: a preliminary result on pervasive nonlinear site effects', *Bull. seism. soc. Am.* **81**, 1859–1884 (1991).
9. B. Gutenberg, 'Effects of ground on earthquake motion', *Bull. seism. soc. Am.* **47**, 221–250 (1957).
10. P. M. Shearer and J. A. Orcutt, 'Surface and near-surface effects on seismic waves—theory and borehole seismometer results', *Bull. seism. soc. Am.* **77**, 1168–1196 (1987).
11. W. D. L. Finn, 'Geotechnical engineering aspects of microzonation', *Proc. 4th int. conf. on seismic zonation*, Stanford, CA, Vol. 1, 1991, pp. 199–259.
12. K. Aki, 'Local site effects on weak and strong ground motions', *Tectonophysics* **218**, 93–111 (1993).
13. S. P. Jarpe, C. H. Cramer, B. E. Tucker and A. F. Shakal, 'A comparison of observations of ground response to weak and strong ground motion at Coalinga, California', *Bull. seism. soc. Am.* **78**, 421–435 (1988).
14. S. K. Singh, J. Lermo, T. Dominguez, M. Ordaz, J. M. Espinosa, E. Mena and R. Quaas, 'The Mexico earthquake of September 19, 1985—a study of amplification of seismic waves in the Valley of Mexico with respect to a hill zone site', *Earthquake spectra* **4**, 653–673 (1988).
15. R. B. Darragh and A. F. Shakal, 'The site response of two rock and soil station pairs to strong and weak ground motion', *Bull. seism. soc. Am.* **81**, 1885–1899 (1991).
16. B. E. Tucker and J. L. King, 'Dependence of sediment-filled valley response on input amplitude and valley properties', *Bull. seism. soc. Am.* **74**, 153–165 (1984).
17. M. Çelebi, 'Topographical and geological amplifications determined from strong-motion and aftershock records of the 3 March 1985 Chile earthquake', *Bull. seism. soc. Am.* **77**, 1147–1167 (1987).
18. S. H. Seale and R. J. Archuleta, 'Site amplification and attenuation of strong ground motion', *Bull. seism. soc. Am.* **79**, 1673–1696 (1989).
19. R. J. Archuleta, S. H. Seale, P. V. Sangas, L. M. Baker and S. T. Swain, 'Garner Valley downhole array of accelerometers: instrumentation and preliminary data analysis', *Bull. seism. soc. Am.* **82**, 1592–1621 (1992).
20. G. Yu, J. G. Anderson and R. Siddharthan, 'On the characteristics of nonlinear soil response', *Bull. seism. soc. Am.* **83**, 218–244 (1993).
21. W. D. L. Finn, 'Dynamic analysis in geotechnical engineering', in J. Lawrence Von Thun (ed.), *Earthquake Engineering and Soil Dynamics. II: Recent Advances in Ground-Motion Evaluation*, ASCE geotechnical special publication 20, 1988, pp. 523–591.
22. I. A. Beresnev and A. V. Nikolaev, 'Experimental investigations of nonlinear seismic effects', *Phys. earth planetary interiors* **50**, 83–87 (1988).
23. P. A. Johnson and K. R. McCall, 'Observation and implications of nonlinear elastic wave response in rock', *Geoph. res. letters* **21**, 165–168, 1994.
24. C.-Y. Chang, M. S. Power, Y. K. Tang and C. M. Mok, 'Evidence of nonlinear soil response during a moderate earthquake', *Proc. 12th intl. conf. on soil mech. and found. eng.*, Rio de Janeiro, Brazil, Vol. 3, 1989, pp. 1927–1930.
25. K.-L. Wen, 'Nonlinear soil response in ground motions', *Earthquake eng. struct. dyn.* **23**, 599–608 (1994).
26. D. G. Anderson and Y. K. Tang, 'Summary of soil characterization program for the Lotung large-scale seismic experiment', *Proc. EPRI/NRC/TPC workshop on seismic soil-structure interaction analysis techniques using data from Lotung, Taiwan, Electric Power Research Institute*, Palo Alto, CA, Vol. 1, 1989, pp. 4-1–4-20.
27. K.-L. Wen and Y. T. Yeh, 'Seismic velocity structure beneath the SMART1 array', *Bull. inst. earth sci. acad. sin.* **4**, 51–72 (1984).
28. N. A. Abrahamson, B. A. Bolt, R. B. Darragh, J. Penzien and Y. B. Tsai, 'The SMART1 accelerograph array (1980–1987), a review', *Earthquake spectra* **3**, 263–287 (1987).
29. I. A. Beresnev, K.-L. Wen and Y. T. Yeh, 'Source, path, and site effects on dominant frequency and spatial variation of strong ground motion recorded by SMART1 and SMART2 arrays in Taiwan', *Earthquake eng. struct. dyn.* **23**, 583–597 (1994).
30. H.-Y. Peng and K.-L. Wen, 'Downhole instrument orientations and near surface Q analysis from the SMART2 array data', *Terrestrial, atmospheric and oceanic sciences* **4**, 367–380 (1993).